Materials Science-Poland, 31(4), 2013, pp. 531-542
http://www.materialsscience.pwr.wroc.pl/
DOI: 10.2478/s13536-013-0132-6

VERSITA

Preparation, characterization and photocatalytic performances of materials based on CS_2-modified titanate nanotubes

HUIQIN AN[1,2], XIAOJING HU[2], BAOLIN ZHU[2], JUANJUAN SONG[2], WEILING ZHAO[2], SHOUMIN ZHANG[2], WEIPING HUANG[2*]

[1]School of Environmental and Chemical Engineering, Tianjin Polytechnic University, Tianjin 300387, China
[2]Tianjin Key Lab of Metal and Molecule-based Material Chemistry and Department of Chemistry, Nankai University, Tianjin 300071, China

CS_2-modified titanate nanotubes (CS_2/TiO_2–NTs) are fabricated by reaction of CS_2 and Ti–O^-Na^+ species on titanate nanotubes. Pb^{2+} ions are coated on the modified nanotubes by ion exchange (Pb/CS_2/TiO_2–NTs). The products are characterized by means of nitrogen adsorption-desorption isotherms at 77 K (BET method), transmission electron microscopy (TEM), X-ray photoelectron spectrometry (XPS), X-ray diffraction (XRD), atomic absorption spectrometry (AAS), and diffuse reflectance spectroscopy (DRS). The photocatalytic performances of the products are evaluated by monitoring their catalytic activities for degradation of methyl orange under UV light irradiation. The effects of calcination temperature and atmosphere on the photocatalytic performance are investigated. The results reveal that the photocatalytic activities of CS_2/TiO_2–NTs and Pb/CS_2/TiO_2–NTs are far higher than that of primary nanotubes, and the optimum calcination temperature is 500 °C under N_2 atmosphere. It is also discovered that physically adsorbed Pb^{2+} ions affect the photocatalytic activity of Pb/CS_2/TiO_2–NTs obviously. The photocatalytic activity of washed Pb/CS_2/TiO_2–NTs is higher than that of the unwashed one under the same thermal treatment and reaction conditions.

Keywords: *titanate nanotubes; CS_2; xanthate; Pb^{2+} ions; photocatalytic performance*

1. Introduction

Titanium dioxide has been widely used in the fields of air purifcation, solar cells, electronics, photocatalysis, sensors and so on [1–8]. TiO_2 nanotubes particularly have attracted considerable attention due to their unique combination of physicochemical [9, 10] and structural [11, 12] properties. The tubular structure, large surface-to-volume ratio, high sedimentation rate are the distinct properties of TiO_2 nanotubes, which make them not only be a good photocatalyst, but also a suitable support for the heterogeneous catalyst [13–16]. However, the photocatalytic oxidation rates of TiO_2 nanotubes for many target hazardous pollutants are too slow to be of practical values [17–19]. The large bandgap [20, 21] and quick recombination of photoinduced charge carriers in TiO_2 [22, 23] result in low photoefficiency of TiO_2 catalyst. Many efforts have been made in order to improve the photocatalytic activity and enhance the photoefficiency of TiO_2. It has been reported that one of efficient methods of enhancing photocatalytic activity of TiO_2 is doping or coupling TiO_2 with metal/non-metal or other semiconductor [24–27]. Among them, non-metal dopants may be more appropriate. Though non-metal dopant does not act as charge carrier, its role as recombination center of charge carriers might be minimized [28]. To date, some non-metal dopants such as nitrogen [29–31], carbon [32–34], sulfur [35–38], phosphorus [39] and halogen atoms [40] etc. have been investigated.

Besides single non-metal doped TiO_2, the multiple-no-metal co-doped TiO_2 has attracted a lot of attention recently [41, 42]. For example, Li et al. have synthesized N–F-co-doped TiO_2 photo-

*E-mail: hwp914@nankai.edu.cn

catalysts by spray pyrolysis using $TiCl_3$ and NH_4F as precursors; the catalysts showed high photocatalytic activity [43]. Luo et al. have prepared Br–Cl-co-doped TiO_2 system and investigated its photocatalytic efficiency for splitting of water into H_2 and O_2 in the presence of Pt co-catalyst and under UV light irradiation [44]. CS_2, a chemical containing two non-metal elements, can be used to synthesize xanthate. Chakraborty et al. have used xanthates prepared via reaction of CS_2 with cellulosic base material to remove copper ions from wastewater [45]. CS_2-modified titanate nanotubes, which were fabricated via reaction of CS_2 with $Ti–O^-Na^+$ species on titanate nanotubes prepared by a hydrothermal treatment in our previous work, contained xanthates and were able to adsorb heavy metal ions in water efficiently [46]. However, the reactivation of the CS_2-modified titanate nanotubes that adsorbed heavy metal ions is difficult, which limits their practical applications. In order to overcome the shortcoming, we provide a comprehensive use of the CS_2-modified titanate nanotubes. Firstly, the CS_2-modified titanate nanotubes are used as adsorbent to remove heavy metal ions in wastewater; then the nanotubes are used as photocatalysts after appropriate treatment, in which the C, S and heavy metal ions become dopants of the titanate nanotubes.

We have decided using CS_2 for two reasons. Firstly, CS_2 can be bound covalently to the surface of titanate nanotubes by O–C bonds, which is distinctly different from other physical adsorption and ordinary doping. Secondly, TiO_2 can be co-doped by two non-metal elements synchronously in a simple process. Previously, we have reported on the performance of CS_2-modified titanate nanotubes in the treatment of wastewater [46], and Jia et al. also reported similar work [47]. When treating wastewater containing Pb^{2+} ions, the CS_2-modified titanate nanotubes adsorb Pb^{2+} ions to form lead xanthate by reaction of Pb^{2+} ions with $Ti–O–C(S)–S^-$. PbS, an important visible-light-sensitive semiconductor with a narrow bandgap, has been widely used in combination with TiO_2 for improving photoefficiency of TiO_2 [48–52]. In the present contribution, we report the photocatalytic performances of materials based on CS_2-modified titanate nanotubes. The effects of calcination temperature and atmosphere on the photocatalytic performances of prepared catalysts are investigated.

2. Experimental

2.1. Materials and characterization

All reagents were analytical grade and used without any further purification.

The morphologies and microstructures of synthesized samples were analyzed by TEM (Philips T20ST). The chemical states of elements in the samples were determined by XPS (PHI-1600 spectrometer equipped with an Mg Kα radiation for exciting photoelectrons), and all binding energies were calibrated using Au 4f7/2 ($E_b = 84.0$ eV) as reference. The phase structures of the samples were characterized with XRD (Rigaku D/Max-2500 X-ray diffractometer with Cu Kα radiation). The bulk compositions of the samples were measured with an atomic absorption spectrometer (AAS, HITACHI 180-80). DRS (UV3600 UV/Vis spectrometer) was used for the measurement of the optical absorption properties of the samples. The specific surface areas of the samples were measured at liquid N_2 temperature using BET method (BET, JW-K).

2.2. Evaluation of photocatalytic activity

A photoreactor (XPS-7 series) was used to test the photocatalytic activities of the samples. Photocatalyst (0.05 g) was dispersed in 100 ml of methyl orange aqueous solution (17 mg/l) in each experiment. The reactor was irradiated with a 300 W high-pressure mercury lamp. At regular time intervals of irradiation, 5 ml of liquid mixture was withdrawn and centrifuged, and the concentration of methyl orange in the clear solution was measured using a TU-1901 UV-Vis spectrometer at 463.8 nm, where methyl orange showed the maximum absorption. The results were corrected for the decomposition of the dye in the absence of catalysts and for adsorption of dye on the catalyst.

2.3. Synthesis of titanate nanotubes

Titanate nanotubes were synthesized via the processes initially developed by Kasuga et al. [53]. Pure anatase TiO_2 powder was dispersed in an aqueous solution of NaOH (10 M) and the mixture was charged into a Teflon-lined autoclave. The autoclave was heated in an oil bath at 150 °C for 12 h. The obtained sample was composed of titanate nanotubes.

2.4. Synthesis of CS_2-modified titanate nanotubes

CS_2-modified titanate nanotubes were fabricated by reaction of CS_2 with titanate nanotubes. In a typical synthesis, the obtained titanate nanotubes were dispersed in pure CS_2 under stirring. The stirring did not stop until the system became a bright yellow color. The product was centrifuged, washed with water, 0.1 M HNO_3 solution and ethanol in turn, and then dried in vacuum overnight. The obtained CS_2-modified titanate nanotubes were calcinated at various temperatures under different atmospheres. The calcinated samples were denoted as CS_2/TiO_2–NTs (T, X), which means that the sample was calcinated at T °C and under X atmosphere.

2.5. Synthesis of $Pb/CS_2/TiO_2$–NTs

In a typical synthesis, the theoretical amount of CS_2/TiO_2–NTs was dispersed in the solution of $Pb(O_2CCH_3)_2$ under stirring for 12 h. The product denoted as $Pb/CS_2/TiO_2$–NTs was collected by centrifuging and divided into two parts. One part was dried in vacuum overnight; the other one was washed with water repeatedly, and then filtered and dried in vacuum overnight. Both of them were calcinated at various temperatures in different atmospheres. The contents of Pb^{2+} ions in the samples were detected by AAS.

3. Results and discussion

3.1. Characterization of CS_2/TiO_2–NTs and $Pb/CS_2/TiO_2$–NTs

CS_2-modified titanate nanotubes were prepared by reaction of CS_2 with titanate nanotubes. The detailed schematic diagram is shown in Fig. 1. As illustrated in Fig. 1, Ti–O–C(S)–S^- forms as a result of the reaction of CS_2 with Ti–O^-Na^+ species on the surface of titanate nanotubes. In a subsequent reaction, Pb^{2+} ions are exchanged onto the surface of CS_2/TiO_2–NT, leading to the formation of $Pb/CS_2/TiO_2$–NTs.

For CS_2/TiO_2–NTs and $Pb/CS_2/TiO_2$–NTs, some characterization results obtained in our previous work are cited here. The IR spectrum and corresponding EDXA spectra confirm the presence of –O–C(S)–S^- species on the surfaces of TiO_2 nanotubes [46].

Fig. 2 shows the TEM images of as-prepared CS_2/TiO_2–NTs and $Pb/CS_2/TiO_2$–NTs. As has been reported [16, 53], titanate nanotubes are open-ended, and have a length of hundreds of nanometers. It can be seen from Fig. 2A that the as-prepared CS_2/TiO_2–NTs is of high quality, and its TEM image is almost consistent with that of titanate nanotubes, which confirms that CS_2 modification takes place only on the surface of nanotube and does not destroy the tubular structure of the titanate nanotube. After Pb^{2+} ions are exchanged on the surface of nanotubes, it can be detected that some black particles adsorb on the outer and inner surfaces of the nanotubes (Fig. 2B,C). They are plumbiferous nanoparticles.

The specific surface areas of titanate nanotubes and as-prepared CS_2/TiO_2–NTs are 241.42 m^2/g and 247.94 m^2/g, respectively, which further confirms that the tubular structure of the nanotubes is intact and not destroyed by CS_2 modification.

3.2. Photocatalytic activities of prepared samples

The photodegradation of methyl orange in aqueous solution was used to evaluate the photocatalytic activities of prepared samples. The effects of calcination temperature, atmosphere and physically adsorbed Pb^{2+} ions on photocatalytic performances are investigated. Detailed discussions are presented in the following sections.

3.2.1. Effect of calcination temperature on photocatalytic activity of CS_2/TiO_2–NTs

Fig. 3 shows the photocatalytic curves of CS_2/TiO_2–NT calcinated at various temperatures

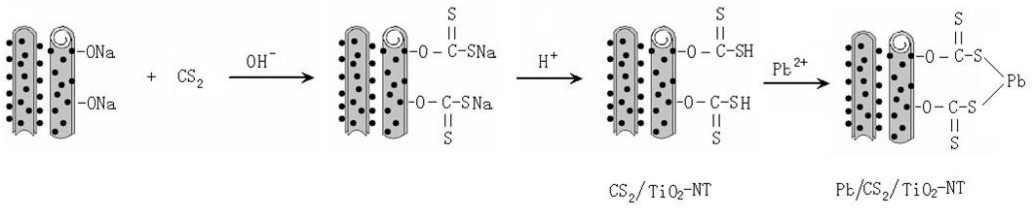

Fig. 1. Schematic diagram of binding of CS_2 to the surface of a TiO_2 nanotube.

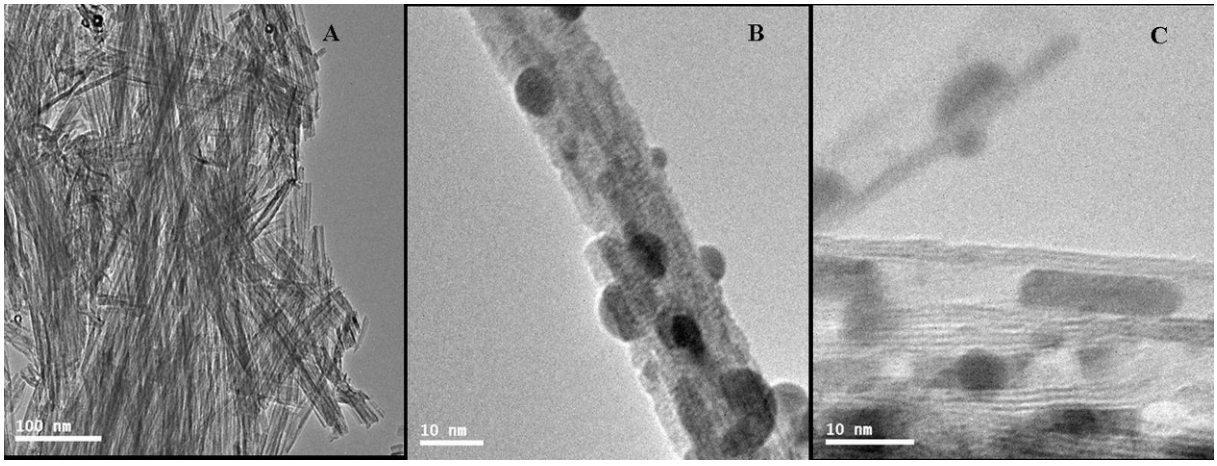

Fig. 2. TEM images of as-prepared CS_2/TiO_2–NTs (A) and $Pb/CS_2/TiO_2$–NTs (B, C).

under N_2 atmosphere, and the catalytic activity of TiO_2–NTs (500 °C, N_2) is also included in Fig. 3 for comparison. Fig. 3A shows clearly that the calcination temperature affects the photocatalytic activity of the sample, which increases with the rise of calcination temperature below 500 °C. The photocatalytic activity of CS_2/TiO_2–NTs (500 °C, N_2) is the highest. As shown in Fig. 3B, under the same reaction conditions, CS_2/TiO_2–NTs (500 °C, N_2) shows higher photocatalytic activity than TiO_2–NTs (500 °C, N_2); about 100 % (Fig. 3B-a) and 70 % (Fig. 3B-b) of the methyl orange is degraded, respectively. It indicates that the photocatalytic activity of the nanotubes is obviously enhanced by CS_2 modifying. In addition, from the inset curves of $\ln(C_0/C)$ vs. irradiation time in Fig. 3, it can be seen that photocatalytic degradation accords with first-order kinetics, $\ln(C_0/C) = kt$. The corresponding k values are listed in Table 1.

It is well known that the photocatalytic activity of TiO_2 is related to the phase structure and specific surface area of TiO_2; the calcination can change the specific surface area and the crystal phase of TiO_2 nanotubes. With the increase in calcination temperature, the micro-structures of samples vary [16, 54], which affects the photodegradation efficiency. The calcination at appropriate temperature can increase the content of anatase phase in a sample, which is beneficial for the increase of photocatalytic activity. However, calcination at too high temperature may not only decrease the specific surface areas of TiO_2 nanotubes or destroy the tubular structure, but also decrease the content of anatase phase in a sample, which might result in the decrease in photodegradation efficiency. During calcination process, a part of C and S on the surfaces of TiO_2 nanotubes can incorporate into the crystalline structure of TiO_2 [55], which is also responsible for the increase in photocatalytic activity. Firstly, the C and S can serve as reductants or convert some Ti^{4+} ions into Ti^{3+} ions. The emergence of Ti^{3+} species results in the formation of surface oxygen vacancies [56–58]. The role of oxygen vacancies is to provide the formation sites of

Table 1. The rate constants (k) of photodegradation of methyl orange solution over TiO_2–NTs (500 °C, N_2) and CS_2/TiO_2–NTs calcinated at different temperatures in N_2 atmosphere.

Sample	CS_2/TiO_2–NTs (N_2)				TiO_2–NTs (N_2)
Temp.	Uncalcinated	300 °C	400 °C	500 °C	500 °C
$k(h^{-1})$	0.3591	0.4072	0.5828	0.7547	0.3806

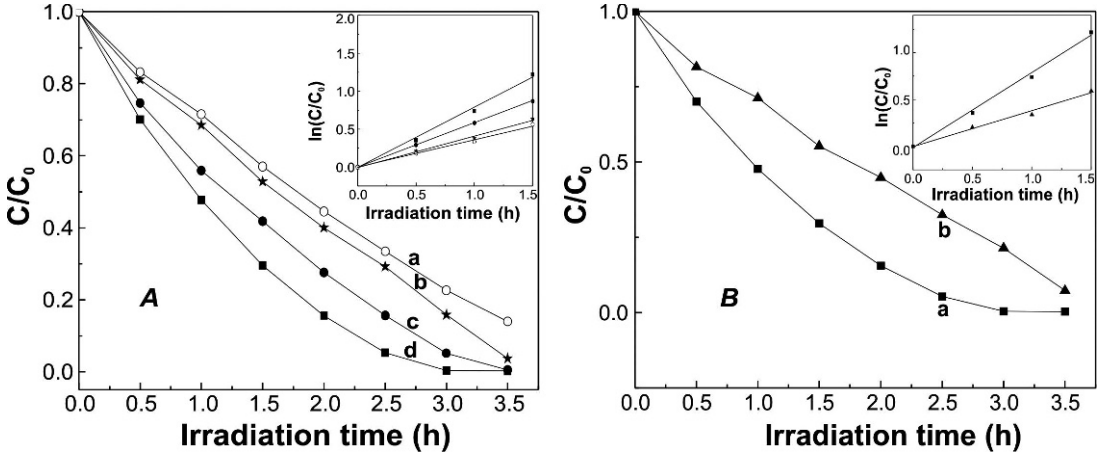

Fig. 3. The photocatalytic activities of samples: (A) CS_2/TiO_2–NTs(N_2): as prepared (a), calcinated at 300 °C (b), 400 °C (c) and 500 °C (A-d, B-a); (B) TiO_2–NTs(500 °C, N_2) (b); inset curves are the corresponding $\ln(C_0/C)$ vs. irradiation time.

active species for photocatalytic reaction and enhance the photocatalytic activity [24]. Secondly, the p-orbitals of these non-metal dopants significantly overlap with the O 2p-orbitals in the valence band, which not only narrows the bandgap of TiO_2, but also facilitates the transport of photogenerated charge carriers to the surface of the catalyst [28, 59, 60]. The narrower bandgap extends the optical response of samples to visible region and facilitates excitation of an electron from the valence band to the conduction band [61], which are beneficial for the enhancing photocatalytic activity too. Though, to some extent, the nanotubular structure of a sample can be destroyed by calcination at 500 °C (see Fig. 9), the treatment conducted at this temperature should be the most efficient because O^{2-} ions in the lattice are replaced under such condition, which results in formation of surface oxygen vacancies and the highest photocatalytic efficiency.

Fig. 4 shows the XRD patterns of TiO_2–NTs (500 °C, N_2) and CS_2/TiO_2–NTs (500 °C, N_2).

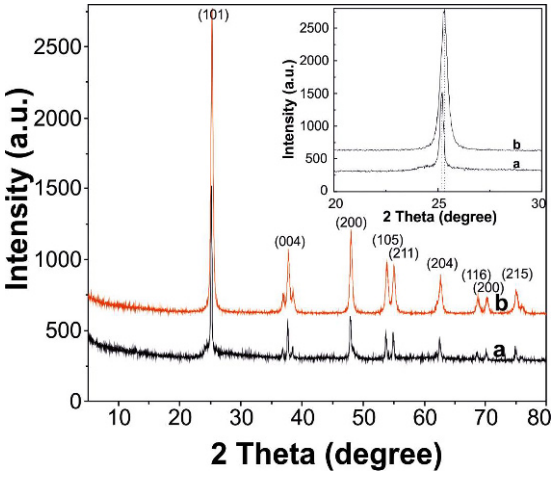

Fig. 4. XRD patterns of TiO_2–NTs (500 °C, N_2) (a) and CS_2/TiO_2–NTs (500 °C, N_2) (b).

Both of them reveal similar diffractions which are attributed to anatase TiO_2, and no additional reflections are observed in the XRD pattern of CS_2/TiO_2–NTs (500 °C, N_2). However, there are still differences between them. The XRD peaks of

the (101) plane of TiO_2–NTs (500 °C, N_2) and CS_2/TiO_2–NTs (500 °C, N_2) are shown in the inset of Fig. 4. Compared with XRD peaks of TiO_2–NTs (500 °C, N_2), the (101) peak of anatase phase of CS_2/TiO_2–NTs (500 °C, N_2) shifts slightly to higher values of 2θ, indicating the surface strain and lattice distortion of CS_2/TiO_2–NTs (500 °C, N_2). After calcination, a part of C and S atoms in the sample may incorporate into the crystalline structure of TiO_2, the adventitious carbon and sulfur replace the O^{2-} ions in the TiO_2 lattice, which leads to the surface strain and lattice distortion of TiO_2 lattice. This conclusion is supported by the results of the calculation of the lattice parameters of two samples. Based on the Bragg law:

$$2d\sin\theta = \lambda \tag{1}$$

and the formula for a tetragonal system:

$$\frac{1}{d^2} = \frac{h^2+k^2}{a^2} + \frac{l^2}{c^2} \tag{2}$$

the lattice parameters of two samples were obtained and listed in Table 2.

Table 2. Lattice parameters of the TiO_2–NTs (500 °C, N_2) and CS_2/TiO_2–NTs (500 °C, N_2).

Lattice Parameter (Å)	*a*	*b*	*c*
TiO_2–NT	3.7832	3.7832	9.8378
CS_2/TiO_2–NT	3.7832	3.7832	9.5507

It can be seen from Table 2 that the lattice parameters remain unchanged along a and b axes. However, there are differences in c-axis parameters, indicating a lattice distortion along the c-axis due to the presence of adventitious carbon and sulfur. Similar conclusion that sulfur and/or carbon result in lattice distortion have been reported [54, 56].

The optical absorption properties of TiO_2–NTs (500 °C, N_2) and CS_2/TiO_2–NTs (500 °C, N_2) were characterized by DRS measurement, and the spectra were recorded at room temperature. Fig. 5 depicts the absorption spectra of TiO_2–NTs (500 ^{o}C, N_2) and CS_2/TiO_2–NTs (500 °C, N_2), respectively. As shown in Fig. 5, the optical absorption band edge of CS_2/TiO_2–NTs (500 °C, N_2) shows a significant red shift compared with that of TiO_2–NTs (500 °C, N_2). The band gap of CS_2/TiO_2–NTs (500 °C, N_2) is ~2.95 eV, which has been estimated from the intercept of UV-Vis diffuse reflectance spectra through a linear extrapolation, and is smaller than that of primary anatase TiO_2 (3.2 eV). After calcination, a part of C and S is doped into the TiO_2 lattice, and then a part of O atoms in the TiO_2 lattice is substituted by C and/or S. The p-orbitals of these dopants overlap with the O 2p-orbitals in valence band, a new impurity level is introduced between the conduction and valence band of TiO_2, and then the electrons can be promoted to the conduction band from the impurity level. Therefore, the bandgap of CS_2/TiO_2–NTs (500 °C, N_2) is narrower than that of pure TiO_2 nanotubes.

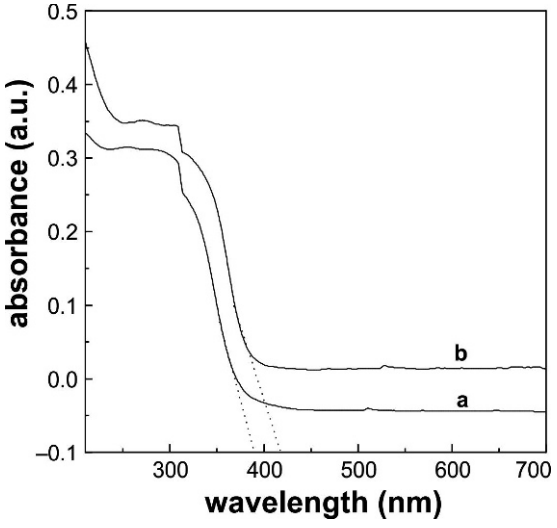

Fig. 5. UV-Vis DRS absorption spectra of TiO_2–NTs (500 °C, N_2) (a) and CS_2/TiO_2–NTs (500 °C, N_2) (b).

XPS was applied to confirm the existence of carbon and sulfur in TiO_2 lattice and investigate the chemical states of dopants in TiO_2. The C_{1s}, S_{2p}, O_{1s}, and Ti_{2p} XPS spectra of CS_2/TiO_2–NTs (500 °C, N_2) are shown in Fig. 6. In Fig. 6A, the strong peak at a binding energy of 285.8 eV arises from elemental carbon [62]; the other peak at 289.8 eV can be assigned to the existence of C–O and C=O bonds of carbonate species [63],

which may be caused by the calcination. Similar results have been reported; for instance, Wang et al. reported the peak of C–O and C=O bonds of carbonate species in the C–N–S–co-doped TiO_2 nanocrystals prepared by a facile hydrothermal method [64]. Sun et al. also detected the existence of C–O and C=O bonds in the C–S-co-doped TiO_2 [54]. The S_{2p} XPS spectrum is shown in Fig. 6B. The sulfur has a peak at about 162.3 eV. It corresponds to the anionic S^{2-} in Ti–S bond in the TiO_2 lattice [65], which suggests that the sulfur only replaces the O^{2-} ions in TiO_2 lattice. No peaks are found around 169, 168 and 166 eV, which correspond to the S^{6+}, S^{4+} and S^{2+} species, respectively. Binding energies of 458.7 and 464.2 eV are attributed to the Ti^{4+} species, and the Ti^{3+} species are indicated by binding energy of 456.9 eV (Fig. 6C). The binding energy difference, $\Delta E_b = 464.2 - 458.7 = 5.5$ eV, is close to 5.7 eV which indicates the standard binding energy for Ti element. The O 1s spectra can be deconvoluted into three component peaks at 530.7, 533.0, and 534.3 eV as shown in Fig. 6D. The peak at 530.7 eV is attributed to crystal lattice O bounded to Ti^{4+} or Ti^{3+} species. The binding energies at 533.0 and 534.3 eV are attributed to the hydroxyl oxygen and adsorbed oxygen or oxygen in the carbonate species, respectively.

3.2.2. Effect of calcination atmosphere on photocatalytic activity of CS_2/TiO_2–NTs

Fig. 7 shows photocatalytic activities of CS_2/TiO_2–NTs calcinated at 500 °C under N_2 and air, respectively. It can be seen from Fig. 7 that the activity of CS_2/TiO_2–NTs (500 °C, N_2) is higher than that of CS_2/TiO_2–NTs (500 °C, air); their k values are 0.7547/h and 0.5720/h, respectively, which indicates that N_2 atmosphere is the optimum calcination atmosphere for photocatalytic activity of CS_2/TiO_2–NTs. Here, the main factor that affects the photocatalytic efficiency is the amount of dopants in TiO_2. When CS_2/TiO_2–NTs is calcinated in air atmosphere, the carbon and sulfur bound covalently to the surface of TiO_2–NTs can react effectively with O_2 to form gaseous oxides in the process of calcination. The escape of the gases reduces the amount of carbon and sulfur in TiO_2–NTs, leading to the decrease in photocatalytic activity of doped TiO_2–NTs.

Fig. 8 is the TEM image of CS_2/TiO_2–NTs (500 °C) calcinated under different atmospheres. Compared with the length of CS_2/TiO_2–NTs (500 °C, N_2) nanotubes (Fig. 8A), the length of the nanotubes shown in Fig. 8B is relatively short, and almost all of the nanotubes are broken and agglomerate, indicating collapse of nanotubular structure. It has been reported that the TiO_2 nanotubes are composed of corrugated ribbons of edge-sharing TiO_6 octahedra [66, 67]. Because of the large specific surface area and surface energy of TiO_2 nanotubes, some unsaturated O may combine with H originated from the water in air atmosphere in the process of calcination, which may result in the breaking of Ti–O bonds and collapse of tubular structure. The collapse leads to the decrease of the specific surface area, and it also adversely affects the photocatalytic activity.

3.2.3. Effect of physically adsorbed Pb^{2+} ions on photocatalytic activity of $Pb/CS_2/TiO_2$–NTs

Pb^{2+} ions are exchanged on the surface of CS_2/TiO_2–NTs by the ion exchange reaction, leading to the formation of $Pb/CS_2/TiO_2$–NTs (Fig. 1). The amount of Pb^{2+} ions in washed and unwashed samples have been detected by AAS and the results are listed in Table 3.

The amounts of Pb^{2+} ions in unwashed and washed nanotubes are 508 mg/g (0.0025 mol/g) and 220 mg/g (0.0011 mol/g), respectively. According to the report by Yang et al. [12], the composition of titanate nanotubes prepared by hydrothermal treatment is $Na_2Ti_2O_4(OH)_2$. The reactions on the surface of the nanotube shown in Fig. 1 can be expressed as follows:

$$Na_2Ti_2O_4(OH)_2 \xrightarrow[(3)Pb(O_2CCH_3)_2]{(1)CS_2,(2)H^+} Ti_2O_2(OH)_2(O\text{–}C(S)\text{–}S)_2Pb. \quad (3)$$

If $Na_2Ti_2O_4(OH)_2$ is completely converted into $Ti_2O_2(OH)_2(O\text{–}C(S)\text{–}S)_2Pb$ after reaction 3, the highest amount of chemically linked Pb^{2+} ions in $Pb/CS_2/TiO_2$–NTs should be 0.0018 mol/g (Ta-

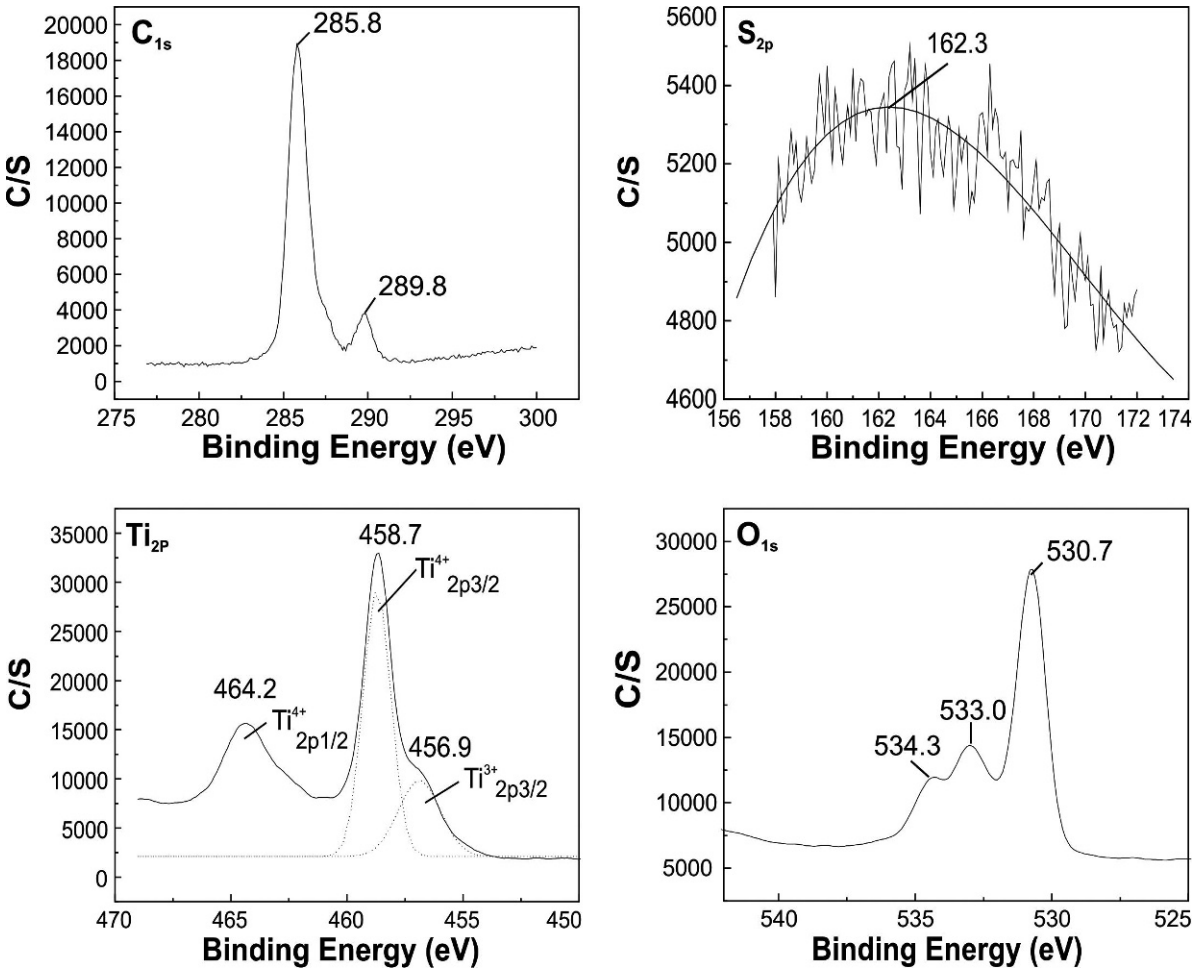

Fig. 6. C_{1s}, S_{2p}, Ti_{2p} and O_{1s} XPS spectra of CS_2/TiO_2–NTs (500 °C, N_2).

ble 3), which is slightly lower than that in unwashed $Pb/CS_2/TiO_2$–NTs (0.0025 mol/g) and higher than that in washed $Pb/CS_2/TiO_2$–NTs (0.0011 mol/g). It indicates that the Pb^{2+} ions not only anchor to nanotubes through chemical bonds but also exist as physically adsorbed ones in unwashed samples. The physically adsorbed Pb^{2+} ions can be removed by washing with water.

Fig. 9 shows the TEM and HR-TEM images of unwashed $Pb/CS_2/TiO_2$–NTs (500 °C, N_2). It can be seen clearly from Fig. 9A that almost no collapse happens in the process of calcination; $Pb/CS_2/TiO_2$–NTs (500 °C, N_2) still has a good morphology after calcination at 500 °C and the length of the nanotubes is up to several hundreds of nanometers. At high magnification (Fig. 9B, C), some black particles deposit can be detected on the outer and inner surfaces of the nanotubes. They are plumbiferous nanoparticles. In the Fig. 9C, there is a crystalline stripe characteristic of plumbiferous nanoparticles (the inset a is the enlarged image of selected region from Fig. 9C). The fringe periodicities of the particles have been measured to be 0.343 and 0.298 nm, respectively, which is consistent with the lattice spacings of (111) and (200) planes of PbS (JCPDF 5-0592). In order to further confirm the structure of the stripe phase, we made Fast Fourier Transformation (FFT) in an area selected from the image (Fig. 9C inset). The in situ electron diffraction displays that the diffraction spot pattern is characteristic of face-centered cubic (FCC) PbS. Hence, it can be further confirmed that the particles deposited on the nanotube are PbS nanocrystals. During calcination, a part of S incor-

Table 3. The contents of Pb^{2+} ions in washed and unwashed samples.

Theoretical content of Pb^{2+} ions by chemical links	Content of Pb^{2+} ions (washed)	Content of Pb^{2+} ions (unwashed)	Content of Pb^{2+} ions physically adsorbed
–	220 mg/g	508 mg/g	288 mg/g
0.0018 mol/g[a]	0.0011 mol/g[b]	0.0025 mol/g[b]	0.0014 mol/g[b]

[a] represents the theoretical mol content of Pb^{2+} ions, and is calculated by the formula: $n = \frac{m}{m \times M_{Ti_2O_2(OH)_2(O-C(S)-S)_2Pb}}$ where m is the quality of $Ti_2O_2(OH)_2(O–C(S)–S)_2Pb$, M is the molecular weight of $Ti_2O_2(OH)_2(O–C(S)–S)_2Pb$

[b] represents the practical molar content of Pb^{2+} ions, and is calculated by the formula: $n = m/M_{Pb}$

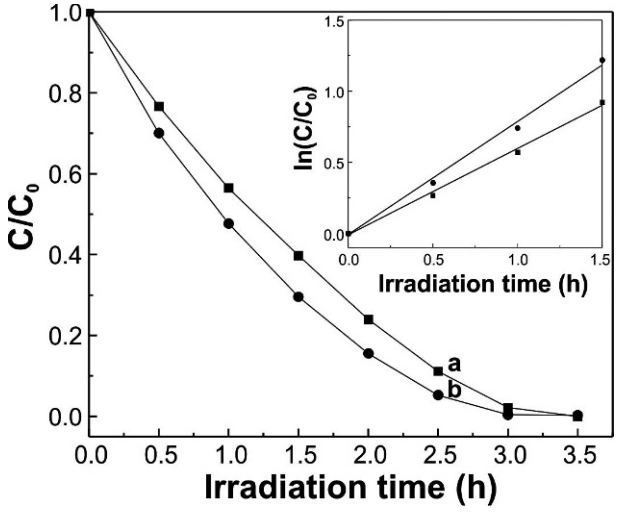

Fig. 7. The photocatalytic activity of CS_2/TiO_2–NTs calcinated at 500 °C in different atmospheres: (a) air, (b) N_2; inset curves are the corresponding $\ln(C_0/C)$ vs. irradiation time.

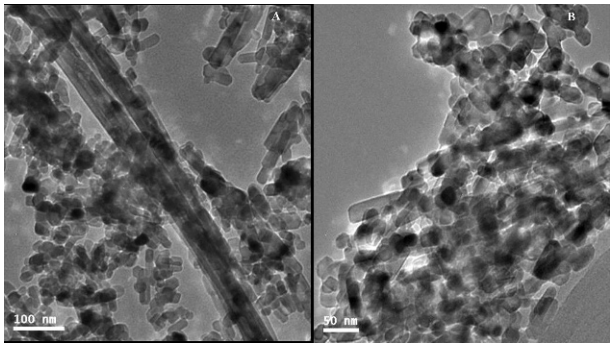

Fig. 8. TEM image of (A) CS_2/TiO_2–NTs (500 °C, N_2) and (B) CS_2/TiO_2–NTs (500 °C, air).

porates into the TiO_2 lattice to replace the O^{2-} ions in TiO_2 lattice, which is supported by XPS discussed above; the remaining S reacts with Pb to form PbS during calcination.

It is well known that titanate nanotubes made by hydrothermal treatment are formed through scrolling the TiO_2 sheet [68]. After binding Pb^{2+} ions to the CS_2/TiO_2–NTs, the ions existing in the space between the layers may form very small plumbiferous nanoparticles which support

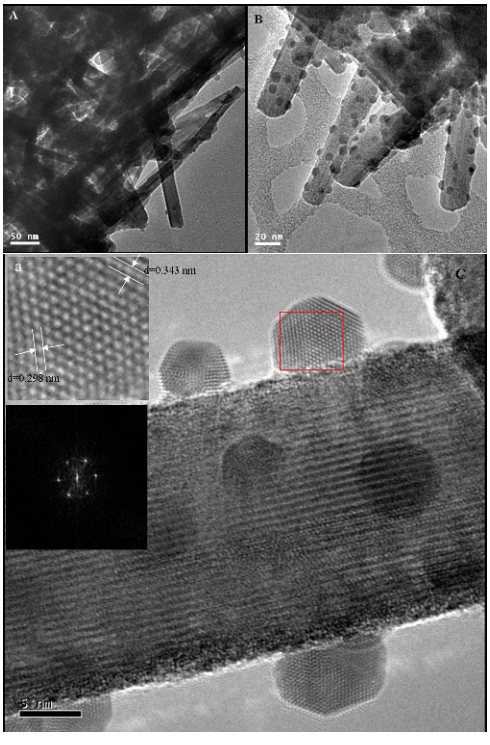

Fig. 9. TEM and HR-TEM images of unwashed $Pb/CS_2/TiO_2$–NTs (500 °C, N_2).

the nanotubular structure and protect the nanotubular structure from destroying while calcination at higher temperature.

Fig. 10 is the HR-TEM image of washed $Pb/CS_2/TiO_2$–NTs (500 °C, N_2). Obviously, plumbiferous nanoparticles are distributed uniformly on the titanate nanotubes because of the formation of PbS on the titanate nanotubes. Compared with Fig. 9, Fig. 10 shows that the size of the plumbiferous nanoparticles on the nanotubes is smaller. During the calcination process, the higher amount of Pb^{2+} ions physically adsorbed on the surface of the unwashed $Pb/CS_2/TiO_2$–NTs resulted in the formation of larger particles containing Pb^{2+} ions.

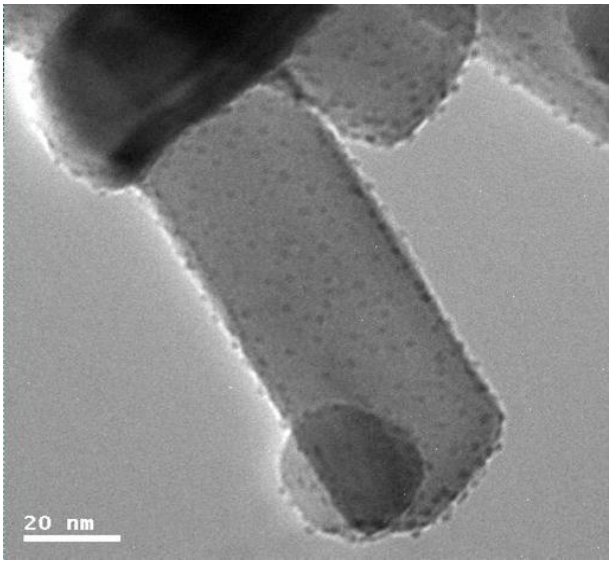

Fig. 10. HR-TEM image of the washed $Pb/CS_2/TiO_2$–NTs (500 °C, N_2).

Table 4. The rate constant (k) of photodegradation of methyl orange solution over washed and unwashed $Pb/CS_2/TiO_2$–NTs calcinated at different temperatures in N_2 atmosphere.

$Pb/CS_2/TiO_2$–NTs (N_2)	Washed	Unwashed		
	500 °C	300 °C	400 °C	500 °C
$k(h^{-1})$	0.7692	0.3083	0.4322	0.5285

Fig. 11 shows the photocatalytic curves of washed $Pb/CS_2/TiO_2$–NTs (500 °C, N_2) and unwashed $Pb/CS_2/TiO_2$–NTs (N_2) calcinated at various temperatures. The corresponding k values are listed in Table 4. As shown in the Fig. 11 and Table 4, the washed $Pb/CS_2/TiO_2$–NTs (500 °C, N_2) exhibits better photocatalytic performance (Fig. 11A-a) than the unwashed one (Fig. 11A-b) and CS_2/TiO_2–NTs (500 °C, N_2) (Fig. 3A-d).

The quantity of Pb^{2+} ions physically adsorbed on the unwashed titanate nanotubes is too large so that they serve as the recombination centers of the photo-generated electrons and holes, resulting in the decrease in photocatalytic activity [69]. Therefore, it is necessary to remove the Pb^{2+} ions physically adsorbed on the surface of a nanotube in order to obtain $Pb/CS_2/TiO_2$–NT photocatalysts with good catalytic performance.

4. Conclusions

1. The covalent attachment of CS_2 to the surface of TiO_2 nanotubes is achieved through a chemical reaction, in which strong Ti–O–C(S)–S^- bonds form as a result of the reaction of CS_2 with the Ti–O^-Na^+ species on the surface. This synthesis process is distinctly different from other physical adsorption and ordinary doping. There are strong covalent bonds between CS_2 and TiO_2 nanotubes, which causes that C and S are more stable on TiO_2 nanotubes and they cannot be removed easily.
2. XPS spectra confirm that non-metals incorporate into the crystalline structure of TiO_2 during a calcination process. By investigating the effects of calcination temperature and atmosphere on the photocatalytic activity of CS_2/TiO_2–NTs, we have found the optimum preparation conditions of TiO_2 photocatalysts containing C and S elements, which is calcination at 500 °C under N_2 atmosphere.
3. $Pb/CS_2/TiO_2$–NTs have been prepared by the reaction of $Pb(O_2CCH_3)_2$ and CS_2/TiO_2–NTs. The photocatalytic performance of washed $Pb/CS_2/TiO_2$–NTs (500 °C, N_2) is better than that of the unwashed one. The results reveal that

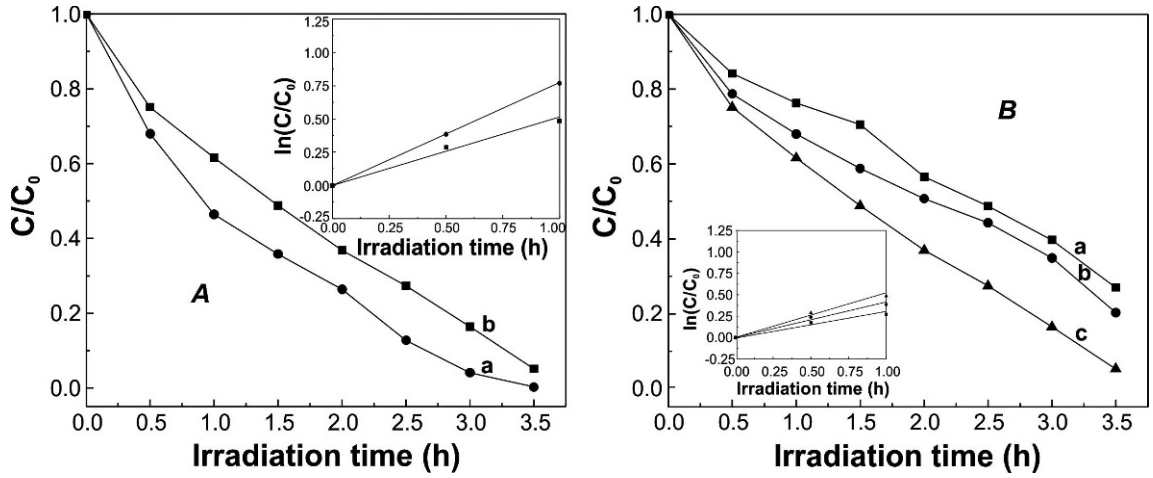

Fig. 11. The photocatalytic activities of washed $Pb/CS_2/TiO_2$–NTs (500 °C, N_2) (A-a) and unwashed $Pb/CS_2/TiO_2$–NTs (N_2) calcinated at 300 °C (B-a), 400 °C (B-b) and 500 °C (A-b, B-c); inset curves are the corresponding $\ln(C_0/C)$ vs. irradiation time.

CS_2/TiO_2–NTs can be used as adsorbent to deal with wastewater containing Pb^{2+} ions, and these nanotubes that adsorbed heavy metal ions can be turned into photocatalysts with a good performance.

Acknowledgements

This work was supported by the National Natural Science Foundation of China (grant number: 21071086), Asian Research Center at Nankai University, the Research Fund for the Doctoral Program of Higher Education (200800551036) and Fundamental Research Funds for the Central Universities (Nankai University 65010031).

References

[1] DAKROURY G., LABIB SH., ABOU-NOUR F.H., *Mater Sci-Poland*, 30 (2012), DOI: 10.2478/s13536-012-0022-3.
[2] HOFFMANN M. R., MARTIN S. T., CHOI W., BAHNEMANN D. W., *Chem Rev*, 95 (1995), 69.
[3] FUJISHIMA A., RAO T. N., TRYK D. A., *J Photochem Photobiol C*, 1 (2000), 1.
[4] CHU S. Z., INOUE S., WADA K., LI D., HANEDA H., AWATSU S., *J Phys Chem B*, 107 (2003), 6586.
[5] BAVYKIN D. V., FRIEDRICH J. M., WALSH F. C., *Adv Mater*, 18 (2006), 2807.
[6] TACHIKAWA T., FUJITSUKA M., MAJIMA T., *J Phys Chem C*, 111 (2007), 5259.
[7] IBHADON A. O., GREENWAY G. M., YUE Y., FALARAS P., TSOUKLERIS D., *Appl Catal B-Environ*, 84 (2008), 351.
[8] TAN A. W., PINGGUAN-MURPHY B., AHMAD R., AKBAR S. A., *Ceram Int*, 38 (2012), 4421.
[9] CHEN X., MAO S. S., *Chem Rev*, 107 (2007), 2891.
[10] BAVYKIN D. V., CRESSEY B. A., LIGHT M. E., WALSH F. C., *Nanotechnology*, 19 (2008), 275604.
[11] CHEN Q., PENG L. M., *Int J Nanotechnol*, 4 (2007), 44.
[12] YANG J. J., JIN Z. S., WANG X. D., LI W., ZHANG J. W., ZHANG S. L., GUO X. Y., ZHANG Z. J., *Dalton T*, 20 (2003), 3898.
[13] IDAKIEV V., YUAN Z. Y., TABAKOVA T., SU B. L., *Appl Catal A-Gen*, 281 (2005), 149.
[14] MOR G. K., SHANKAR K., PAULOSE M., VARGHESE O. K., GRIMES C. A., *Nano Lett*, 6 (2006), 215.
[15] ZHU B. L., GUO Q., HUANG X. L., WANG S. R., ZHANG S. M., WU S. H., HUANG W. P., *J Mol Catal A*, 249 (2006), 211.
[16] AN H. Q., ZHU B. L.. LI J. X., ZHOU J., WANG S. R., ZHANG S. M., WU S. H., HUANG W. P., *J Phys Chem C*, 112 (2008), 18772.
[17] LINSEBIGLER A. L., LU G. Q., YATES J. T., *Chem Rev*, 95 (1995), 735.
[18] DIEBOLD U., *Surf Sci Rep*, 48 (2003), 53.
[19] DENG L. X., WANG S. R., LIU D. Y., ZHU B. L., HUANG W. P., WU S. H., ZHANG S. M., *Catal Lett*, 129 (2009), 513.
[20] LI D. Z., HUANG H. J., CHEN X., CHEN Z. X., LI W. J., YE D., FU X. Z., *J Solid State Chem*, 180 (2007), 2630.
[21] COLMENARES J. C., ARAMENDÍA M. A., MARINAS A., MARINAS J. M., URBANO F. J., *Appl Catal A-Gen*, 306 (2006), 120.
[22] ILIEV V., TOMOVA D., BILYARSKA L., ELIYAS A., PETROV L., *Appl Catal B-Environ*, 63 (2006), 266.
[23] WANG Y. Q., CHENG H. M., ZHANG L., HAO Y. Z., MA J. M., XU B., LI W. H., *J Mol Catal A*, 151 (2000), 205.
[24] YU Y., WU H. H., ZHU B. L., WANG S. R., HUANG W. P., WU S. H., ZHANG S. M., *Catal Lett*, 121 (2008), 165.

[25] CARVALHO HUDSON W. P., BATISTA ANA P. L., PETER H., RAMALHO TEODORICO C. P., *J Hazard Mater*, 184 (2010), 273.
[26] LI H., ZHU B. L., FENG Y. F., WANG S. R., ZHANG S. M., HUANG W. P., *J Solid State Chem*, 180 (2007), 2136.
[27] ZHU B. L., LI K. R., ZHOU J., WANG S. R., ZHANG S. M., WU S. H., HUANG W. P., *Catal Commun*, 9 (2008), 2323.
[28] WANG H., LEWIS J. P., *J Phys-Condens Mat*, 18 (2006), 421.
[29] NOSAKA Y., MATSUSHITA M., NISHINO J., NOSAKA A. Y., *Sci Tech Adv Mater*, 6 (2005), 143.
[30] SHAO G. S., ZHANG X. J., YU Z .Y., *Appl Catal B-Environ*, 82 (2008), 208.
[31] ASAHI R., MORIKAWA T., OHWAKI T., AOKI K., TAGA Y., *Science*, 293 (2001), 269.
[32] IM J. H., YANG S. J., YUN C. H., PARK C.R., *Nanotechnology*, 23 (2012), 035604.
[33] CARPIO E., ZUNIGA P., PONCE S., SOLIS J., RODRIGUEZ J., ESTRADA W., *J Mol Catal A*, 228 (2005), 293.
[34] KHAN S. U. M., AL-SHAHRY M., INGLER JR W. B., *Science*, 297 (2002), 2243.
[35] UMEBAYASHI T., YAMAKI T., TANAKA S., ASAI K., *Chem Lett*, 32 (2003), 330.
[36] OHNO T., AKIYOSHI M., UMEBAYASHI T., ASAI K., MITSUI T., MATSUMURA M., *Appl Catal A-Gen*, 265 (2004), 115.
[37] TIAN F. H., LIU C. B., *J Phys Chem B*, 110 (2006), 17866.
[38] YU H .F., *J Phys Chem Solids*, 68 (2007), 600.
[39] HONG X. T., WANG Z. P., CAI W. M., LU F., ZHANG J., YANG Y. Z., MA N., LIU Y., *J Chem Mater*, 17 (2005), 1548.
[40] YANG G., JIANG Z., SHI H., JONES M. O., XIAO T., EDWARDSB P. P., YANA Z., *App Catal B-Environ*, 96 (2010), 458.
[41] HAMAL D. B., KLABUNDE K. J., *J Colloid Interf Sci*, 311 (2007), 514.
[42] LI D., OHASHI N., HISHITA S., KOLODIAZHNYI T., HANEDA H., *Solid State Chem*, 178 (2005), 3293.
[43] LI D., HANEDA H., HISHITA S., OHASHI N., *Chem Mater*, 17 (2005), 2596.
[44] LUO H., TAKATA T., LEE Y., ZHAO J., DOMEN K., YAN Y., *Chem Mater*, 16 (2004), 846.
[45] CHAKRABORTY S., TARE V., *Bioresource Technol*, 97 (2006), 2407.
[46] AN H. Q., ZHU B. L., WU H. Y., ZHANG M., WANG S. R., ZHANG S. M., WU S. H., HUANG W. P., *Chem J Chinese U*, 29 (2008), 439.
[47] ZHAO X., JIA Q., SONG N., ZHOU W., LI Y., *J Chem Eng Data*, 55 (2010), 4428.
[48] VOGEL R., HOYER P., WELLER H., *J Phys Chem-US*, 98 (1994), 3183.
[49] PATIL R., LOKHANDE C., MANE R., GUJAR T., HAN S., *J Non-Cryst Solids*, 353 (2007), 1645.
[50] HONG J., CHOI D., KANG M., KIM D., KIM K., *J Photoch Photobio A*, 143 (2001), 87.
[51] CHEN S., PAULOSE M., RUAN C., MOR G., VARGHESE O., KOUZOUDIS D., GRIMES C., *J Photoch Photobio A*, 177 (2006), 177.
[52] ZHUKOVSKIY M. A., STROYUK A. L., SHVALAGIN V. V., SMIRNOVA N. P., LYTVYN O. S., EREMENKO A. M., *J Photoch Photobio A*, 203 (2009), 137.
[53] KASUGA T., HIRAMATSU M., HOSON A., SEKINO T., NIIHARA K., *Langmuir*, 14 (1998), 3160.
[54] SUN H. Q., BAI Y., CHENG Y. P., JIN W. Q., XU N. P., *Ind Eng Chem Res*, 45 (2006), 4971.
[55] ZHOU M. H., YU J. G., *J Hazard Mater*,152 (2008), 1229.
[56] SHAO G. S., LIU L., MA T. Y., WANG F. Y., REN T. Z., YUAN Z. Y., *Chem Eng J*, 160 (2010), 370.
[57] LI Y. Z., HWANG D. S., LEE N. H., KIM S. J., *Chem Phys Lett*, 404 (2005), 25.
[58] DU X. Y., WANG Y., MU Y. Y., GUI L. L., WANG P., TANG Y. Q., *Chem Mater*, 14 (2002), 3953.
[59] TACHIKAWA T., TOJO S., KAWAI K., ENDO M., FUJITSUKA M., OHNO T., NISHIJIMA K., MIYAMOTO Z., MAJIMA T., *J Phys Chem B*, 108 (2004), 19299.
[60] YANG X. X., CAO C. D., ERICKSON L., HOHN K., MAGHIRANG R., KLABUNDE K., *Appl Catal B-Environ*, 91 (2009), 657.
[61] ZHANG S. M., CHEN Y. Y., YU Y., WU H. H., WANG S. R., ZHU B. L., HUANG W. P., WU S. H., *J Nanopart Res*, 10 (2008), 871.
[62] SAKTHIVEL S., KISCH H., *Angew Chem Int Edit*, 42 (2003), 4908.
[63] PAPIRER E., LACROIX R., DONNET J. B., NANSE G., FIOUX P. CHLORINATION, *Carbon*, 33 (1995), 63.
[64] WANG Y., HUANG Y., HO W., ZHANG L., ZOU Z., LEE S., *J Hazard Mater*, 169 (2009), 77.
[65] LI H. X., ZHANG X. Y., HUO Y. N., ZHU J., *Environ Sci Technol*, 41 (2007), 4410.
[66] MA R., BANDO Y., SASAKI T., *Chem Phys Lett*, 380 (2003), 577.
[67] CHEN Q., ZHOU W. Z., DU G. H., PENG L. M., *Adv Mater*, 14 (2002), 1208.
[68] ZHANG M., JIN Z. S., ZHANG J. W., GUO X. Y., YANG J. J., LI W., WANG X. D., ZHANG Z. J., *J Mol Catal A*, 217 (2004), 203.
[69] ZHANG Z., WANG C. C., ZAKARIA R., YING J. Y., *J Phys Chem B*, 102 (1998), 10871.

Received 2012-08-29
Accepted 2013-07-26